Quantitative Perfusion and Permeability Biomarkers in Brain Cancer from Tomographic CT and MR Images

Libertas Academica
FREEDOM TO RESEARCH

Supplementary Issue: Biomarkers and their Essential Role in the Development of Personalised Therapies (A)

Armin Eilaghi[1–4], Timothy Yeung[5], Christopher d'Esterre[1–4], Glenn Bauman[5], Slav Yartsev[5], Jay Easaw[6], Enrico Fainardi[7,8], Ting-Yim Lee[5] and Richard Frayne[1–4]

[1]Department of Radiology, University of Calgary, Calgary, AB, Canada. [2]Department of Clinical Neurosciences, University of Calgary, Calgary, AB, Canada. [3]Hotchkiss Brain Institute, University of Calgary, Calgary, AB, Canada. [4]Seaman Family MR Centre, Foothills Medical Centre, Calgary, AB, Canada. [5]Lawson Health Research Institute and Robarts Research Institute, London, ON, Canada. [6]Department of Oncology, University of Calgary, Calgary, AB, Canada. [7]Neuroradiology Unit, Department of Neurosciences and Rehabilitation, Azienda Ospedaliero-Universitaria, Arcispedale S. Anna, Ferrara, Italy. [8]Neuroradiology Unit, Department of Radiology, Azienda Ospedaliero-Universitaria Careggi, Firenze, Italy.

ABSTRACT: Dynamic contrast-enhanced perfusion and permeability imaging, using computed tomography and magnetic resonance systems, are important techniques for assessing the vascular supply and hemodynamics of healthy brain parenchyma and tumors. These techniques can measure blood flow, blood volume, and blood–brain barrier permeability surface area product and, thus, may provide information complementary to clinical and pathological assessments. These have been used as biomarkers to enhance the treatment planning process, to optimize treatment decision-making, and to enable monitoring of the treatment noninvasively. In this review, the principles of magnetic resonance and computed tomography dynamic contrast-enhanced perfusion and permeability imaging are described (with an emphasis on their commonalities), and the potential values of these techniques for differentiating high-grade gliomas from other brain lesions, distinguishing true progression from posttreatment effects, and predicting survival after radiotherapy, chemotherapy, and antiangiogenic treatments are presented.

KEYWORDS: brain cancer, perfusion imaging, permeability imaging, quantitative MR and CT techniques

SUPPLEMENT: Biomarkers and their Essential Role in the Development of Personalised Therapies (A)

CITATION: Eilaghi et al. Quantitative Perfusion and Permeability Biomarkers in Brain Cancer from Tomographic CT and MR Images. *Biomarkers in Cancer* 2016:8(S2) 47–59 doi:10.4137/BIC.S31801.

TYPE: Review

RECEIVED: August 19, 2015. **RESUBMITTED:** November 3, 2015. **ACCEPTED FOR PUBLICATION:** November 6, 2015.

ACADEMIC EDITOR: Barbara Guinn, Editor in Chief

PEER REVIEW: Three peer reviewers contributed to the peer review report. Reviewers' reports totaled 524 words, excluding any confidential comments to the academic editor.

FUNDING: The authors acknowledge the support of the Canadian Institutes for Health Research (CIHR); the Medical Imaging Trials Network of Canada (MITNEC), funded by the CIHR; the University of Calgary Eye's high postdoctoral scholar program; the Heart and Stroke Foundation of Canada Fellow program; and the International and Industrial Imaging Training (I3T) program, funded by the Natural Science and Engineering Research Council of Canada Collaborative Research and Training Experience (NSERC CREATE) program. The authors confirm that the funders had no influence over the study design, content of the article, or selection of this journal.

COMPETING INTERESTS: RF discloses royalty payments from Wisconsin Alumni Research Foundation (WARF) for a time-resolved MR imaging technique that could be used for DCE MR imaging, as discussed in this paper. RF holds a patent related to the same, licensed to WARF. TY-L discloses royalties received from licensing of CT perfusion software to GE Healthcare. JE, EF, TY, SY, GB, AE and CdE disclose no potential conflicts of interest.

CORRESPONDENCE: rfrayne@ucalgary.ca

Paper subject to independent expert single-blind peer review. All editorial decisions made by independent academic editor. Upon submission manuscript was subject to anti-plagiarism scanning. Prior to publication all authors have given signed confirmation of agreement to article publication and compliance with all applicable ethical and legal requirements, including the accuracy of author and contributor information, disclosure of competing interests and funding sources, compliance with ethical requirements relating to human and animal study participants, and compliance with any copyright requirements of third parties. This journal is a member of the Committee on Publication Ethics (COPE).

Published by Libertas Academica. Learn more about this journal.

Introduction

Each year, over 250,000 primary brain and central nervous system cancers are diagnosed worldwide, 10% of which occur in North America.[1] These types of cancer have 60% probability of death,[2] and quality of life is often seriously diminished, even in treated patients.[3] Gliomas, tumors derived from neuroglia, represent a majority of primary brain cancer cases. Based on their pathological features determined after biopsy, the World Health Organization (WHO) classifies gliomas into the following four grades: Grade I (low proliferative) and Grade II (infiltrative) are considered low-grade gliomas, whereas Grade III (histological evidence of malignancy) and Grade IV (cytologically malignant, mitotically active, and necrosis-prone neoplasms) are high-grade gliomas.[4,5] While low-grade gliomas may be managed with observation or surgery alone, higher grade tumors typically require multimodality treatment. Current strategies include maximum safe surgical resection followed by radiotherapy and chemotherapy.[6] Although there is evidence that favorable outcome is associated with near-total resection of the tumor, a high-grade, malignant glioma often cannot be completely removed.[7] Even with complete resection, rapid recurrence after surgery alone is common, and adjuvant radiotherapy is typically added to delay the time of recurrence. However, radiation toxicity to the surrounding normal tissue has to be minimized, and thus, the radiotherapy target tissue volume often has to be restricted. Typically, the applied radiation field is optimized using three-dimensional conformal radiotherapy,[8] intensity-modulated radiotherapy,[9] or stereotactic surgery[10] approaches. Such precision radiotherapy techniques require accurate tumor boundary delineation, typically on the basis of standard contrast-enhanced magnetic resonance (MR) imaging. Complementary functional imaging

information better identifies biologically significant tumor volumes (including quantitative perfusion and permeability surface data), enhances the treatment planning process,[11] optimizes treatment decision-making,[12] and enables monitoring of the treatment[13] noninvasively, resulting in improved patient care and treatment outcome.

The growing tumor. Neovascularization and necrosis are biologic hallmarks of malignant glioma that can potentially be interrogated through perfusion imaging. Tumor growth is dependent on the availability of an abundant supply of oxygen and nutrients made possible by efficient blood flow (BF). In primary and metastatic brain tumors, the integrity of the blood–brain barrier (BBB) is compromised.[14] The number of pericytes,[15] astrocytes,[16] and tight junction proteins[17] are reduced, affecting the structural integrity and vascular function of BBB. In addition to BBB dysfunction, decreased tissue oxygen concentration (hypoxia) is another characteristic of rapid tumor growth.[18] Once the tumor has grown beyond the limit of oxygen diffusion (a few millimeters), the normal supply of blood cannot meet the oxygen demands caused by the elevated proliferative state of the tumor.[19] To address this need, an adequate blood supply is provided through several mechanisms including co-option, angiogenesis, and vasculogenesis.[20] These tissue perfusion and/or vessel permeability altering mechanisms are correlated with histopathologic changes and molecular markers related to tumor growth (eg, vascular endothelial growth factor [VEGF]) and, therefore, could be used as a biomarker of tumor malignancy, margin, and invasion.[21]

Tumor identification and assessment. Histopathology remains the gold standard to identify and quantify the extent of a potentially malignant tumor; however, its application and ability to correctly define tumor grade is limited due to the invasive nature of the technique and potential sampling bias.[22] Tomographic (or cross-sectional) imaging-based techniques provide anatomical and functional information throughout the tumor, reducing sampling bias, and are minimally invasive.

The McDonald criteria[23] is perhaps the most well-known metric to evaluate glioblastoma (GBM) treatment response. It uses the product of the maximal orthogonal diameters of the enhancing tumor on T1-weighted MR as a measure of tumor volume.[23] With the introduction of new systemic therapy agents such as temozolomide and bevacizumab, novel patterns of imaging response such as pseudoprogression and pseudoresponse, reflecting treatment-related vascular changes, have emerged, requiring new imaging approaches to assess tumor response.[24–26] The Response Assessment in Neuro-Oncology (RANO) group updated the McDonald criteria in 2010, and the revised document[26] suggests that specific functional imaging techniques, particularly perfusion and permeability, are needed to more appropriately characterize tumor progression and treatment response. Such information can be obtained from computed tomography (CT) or MR imaging, which acquire cross-sectional images that can define the location and size of the tumor. Of particular interest is extravasation of a contrast agent from the leaky BBB, as well as perfusion differences between the rim and core of the tumor. These concepts are described in detail in the following section.

Image-based Measurement of Perfusion and Permeability

A number of tomographic imaging techniques have been used for quantitative measurement of perfusion and permeability including MR-based (1) dynamic contrast-enhanced (DCE), (2) arterial spin labeling (ASL), and (3) dynamic susceptibility contrast (DSC) imaging, as well as (4) CT-based DCE imaging. All the approaches rely on endogenous (ASL) or exogenous agents (DSC, DCE). Exogenous agents are commonly termed contrast (agent) or tracer. For all techniques, quantitative maps are produced from the tomographic image data by applying the principles derived from indicator-dilution theory or kinetic modeling.[24,25] The acquisition requirements for these approaches have been recently reviewed.[27]

Briefly, MR ASL selectively labels arterial blood (ie, it uses an endogenous tracer) in the neck and uses a subtraction imaging technique to assess BF in the brain tissue. ASL is a technology that is gaining interest in neuro-oncology,[28] since it does not require the injection of exogenous contrast agent and does not use radiation. It has been proposed[29] for assessing tumors but is not widely used, though it may have a role in posttherapy surveillance imaging or in patients unable to receive exogenous contrast agents.[27] The main challenges of the ASL technique include rapid T1 decay of the ASL measurements, limiting investigation to where the flow is fast and lower signal-to-noise ratio and spatial resolution compared with DCE and DSC. Also, ASL cannot be performed after injection of T1 contrast agents.[30] A number of different implementations of ASL are currently under assessment including continuous ASL, pulsed ASL, pseudocontinuous ASL, and velocity-selective ASL. Recently, a working group reviewed these emerging clinical techniques and published advice on the standardization of the ASL method, hopefully leading to improved clinical applications of this technique in future.[31]

MR DSC and DCE approaches are conceptually similar except that different MR acquisition techniques are used that cause the measured signal to either decrease or increase, respectively, with increasing contrast agent concentration. In DSC approaches, depending on contrast agent concentration, a susceptibility gradient is generated between the tissue and the vasculature, which decreases the T2*-weighted signal.[32] DSC MR technique is based on the assumptions that the contrast agent dilution in the blood is a function of BF and blood volume (BV) and that contrast agent remains intravascular (ie, does not leak into brain parenchyma) during imaging.[32,33] Challenges when deriving quantitative maps from MR DSC data are numerous and principally derive from the nonlinear relationship between contrast agent concentration and measured signal, which lead to nonstationary noise characteristics[34] and difficulties with partial volume correction.[35] Also, any leakage of the contrast

agent to parenchymal tissue results in violation of the DSC MR assumption and can underestimate BV, particularly when contrast leakage is high, for example, due to damaged BBB as is common with brain tumors.[36] Both ASL and DSC approaches are typically implemented using an echo-planar imaging sequence, which is sensitive to geometric distortions. Furthermore, MR ASL or DSC approaches cannot estimate permeability directly. While there have been efforts to derive *surrogate* measures of permeability from DSC approaches, for example, relative recirculation,[37] the validation of such efforts have been done using direct measurements from DCE approach.

Herein, we concentrate on CT and MR DCE techniques, specifically focusing on their common features. These two approaches are also most commonly used for studying tumor perfusion and are the only MR and CT approaches that are able to estimate permeability. MR and CT DCE imaging characterizes tissue hemodynamics by tracking the passage of a bolus of contrast agent as it traverses through the microvasculature and brain parenchymal tissue. In both modalities, the passage of the contrast agent leads to a corresponding time-course of signal enhancement that can be analyzed.

Kinetic modeling to quantify hemodynamics and BBB permeability surface. MR DCE analysis techniques consist of three main kinetic modeling steps, whereas the corresponding CT analysis only requires the last step[38]:

1. Image signal intensity is converted to contrast agent concentration to obtain the time–concentration curve, $C_t(t)$, of brain tissue or tumor,
2. Image signal intensity from an artery supplying the brain tissue is similarly converted to produce and estimate the arterial input function, $C_a(t)$, and
3. An appropriate tracer kinetic model is then employed to calculate the hemodynamic parameters of interest, such as BF, BV, transit time, and permeability surface area product (PS). (Parenthetically, similar modeling approaches can be used to analyze DSC MR data except for PS).[27,39]

Typically, tissue signals are obtained from all pixels in the brain, including the healthy tissue, so that maps of regional hemodynamic parameters can be obtained. The arterial input function is selected to best correspond to the time–concentration curve of contrast agent entering the tissue(s) of interest. Key tracer kinetic parameters' definitions are summarized in Table 1.

The tissue time–concentration curve, $C_t(t)$, can be mathematically expressed as a convolution between the arterial input function and the blood flow-scaled impulse residue function, $R(t)$ as explained in Ref. 24:

$$C_t(t) = BF \cdot C_a(t) \otimes R(t) = C_a(t) \otimes BF \cdot R(t) \qquad (1)$$

After convolution, this yields an expression for the tissue time–concentration curve.

$$C_t(t) = \int_0^t C_a(t) \cdot [BF \cdot R(t-\tau)] d\tau$$

The impulse residue function, $R(t)$, describes the tissue time–concentration curve when the arterial input function is a delta impulse (ie, a nonphysiologic infinitely tall and narrow bolus), ie, $\frac{1}{BF}\delta(t)$. Empirically, the impulse residue function is the fraction of contrast agent that remains in the tissue as a function of time after injection of an impulse contrast agent into the arterial input. By definition, $\max(R(t)) = 1$ and the impulse residue function decreases monotonically from this maximum with increasing time. Also, $R(t) = 0$ for $t < t_o$, that is before the contrast arrives in the brain tissue at $t = t_o$.

Perfusion quantification. In practice, contrast agent is injected intravenously over a period of time (typically over 15–25 seconds for CT, <10 seconds for MR), such that the arterial input function, $C_a(t)$, is not an impulse, but rather distributed over a finite duration. Provided that the image signal varies linearly with concentration (as is the case for CT and MR DCE) and BF is constant within the period of measurement, the tissue time–concentration curve, $C_t(t)$, can be estimated by the convolution of the arterial input function, $C_a(t)$, and the impulse residue function, $R(t)$, using the mathematical principle of linear superposition, ie, using Eq (1).[24] Total DCE data acquisition duration is normally less than two minutes if only perfusion parameter estimates are required by deconvolution of Eq (1).[24,40] From the deconvolved impulse residue function, BF equals to the maximum of the impulse residue function, while BV can be estimated from the area under the curve of the tissue time–concentration curve as discussed by Lee et al.[24] An acquisition temporal resolution of one to two seconds is typically required to produce perfusion maps.[41]

A commonly used semiquantitative parameter in brain cancer imaging is the normalized BV (nBV). The nBV is defined as the BV in the tumor divided by the BV in the same volume of normal contralateral brain. Peak height (PH) is another semiquantitative measure defined as the maximum contrast enhancement from the baseline signal during the first pass of contrast agent. Normalized blood flow (nBF) and normalized peak height (nPH) of the tumor are defined similar to nBV.

Permeability quantification. If the permeability parameter estimates are of interest (eg, the rate of extravasation of contrast agent from the intravascular space into the extravascular extracellular space (EES) as assessed by PS or K^{trans}), then tomographic imaging data must be collected for longer periods, typically for between three and six minutes.[40] Kinetic models are required to quantify perfusion and permeability parameters.[42] The different kinetic models include the following: (1) model-independent approaches for BF measurements based on the Fick principle and deconvolution

Table 1. Glossary of perfusion and permeability imaging parameters.

TERM	SYMBOL	DEFINITION
Blood flow	BF	Flow rate of the blood per unit mass or volume of tissue (ml.min.100 g^{-1} or ml·min.100 ml^{-1}).
Blood volume	BV	Volume of flowing blood within vasculature per unit mass or volume of tissue (ml.100 g^{-1} or ml.100 ml^{-1}).
Extraction fraction	*E*	Fraction of the contrast that extravasates from intravascular space into extravascular space within the first pass through the vasculature.
Initial AUC	iAUC	A semi-quantitative measure of contrast enhancement used in DCE MR. It is related to dose of contrast injected, the blood volume, and blood–brain barrier permeability surface product.
Mean $AUCR_H$	$mAUCR_H$	The ratio between iAUC and the final AUC from a DCE MR scan gives AUCR. If the histogram of AUCR of a region is bimodal or skewed, the mean for higher peak of this distribution is calculated to give the $mAUCR_H$.
Mean transit time	MTT	Average time(s) for blood to traverse from arterial to the venous end of the vasculature.
Normalized BF	nBF	BF of a region of interest normalized to the contralateral normal brain.
Normalized BV	nBV	BV of a region of interest normalized to the contralateral normal brain.
Normalized maximum slope	–	A semi-quantitative estimation of BF. It is the maximum slope of a tissue time-contrast enhancement curve normalized by the maximum of the arterial time-contrast enhancement curve.
Peak height	PH	A measure of maximum contrast enhancement from the baseline signal during the first pass of contrast.
Normalized peak height	nPH	PH of the tumor can be normalized to the contralateral normal brain to give the normalized peak height.
Permeability	–	Unidirectional flux rate of contrast agent from the blood plasma into the brain parenchyma (ie, interstitial space) normalized by the total surface area of capillaries per unit mass of tissue. It is often estimated using the parameters permeability-surface area product (PS) and transfer rate constant (K^{trans}).
Permeability surface area product	PS	Product of permeability and total surface area of capillaries per unit mass of tissue (ml.min.100 g^{-1}).
Efflux rate constant	k_{ep}	Rate constant of contrast efflux rate from the brain parenchyma back into the blood plasma (min^{-1}).
Transfer constant	K^{trans}	Flow rate constant of contrast from the blood plasma to the brain parenchyma (min^{-1}).
Vp	Vp	Volume of flowing blood within the vasculature per unit mass or volume of tissue (ml.100 g^{-1} or dimensionless).
Extravascular volume	v_e	Volume of extracellular space per unit volume of tissue for contrast to distribute into (ml.100 g^{-1} or dimensionless).

analysis; (2) compartmental modeling, as exemplified by the Patlak model;[43] or (3) modeling that accounts for convective transport (BF) and bidirectional diffusion exchange (capillary permeability) via a distributed parameter model, eg, the Johnson–Wilson model.[44] Both compartmental and distributed parameter models have been used to calculate kinetic parameters including BF, BV, and PS from DCE images.

Here, we focus on the Johnson–Wilson model,[44] in particular, its modification by St Lawrence and Lee.[45] The modified Johnson–Wilson model is a more physiologically realistic distributed parameter model and allows the simultaneous determination of BF, BV, and PS. The modified Johnson–Wilson model has a closed-form solution to the impulse residue function $R(t)$.[45] $R(t)$ is defined as:

$$R(t) = \begin{cases} 1 & 0 < t \le \frac{BV}{BF} \\ Ee^{-\frac{BF \cdot E}{v_e}\left(t - \frac{BV}{BF}\right)} & t > \frac{BV}{BF} \end{cases}, \qquad (2)$$

where the extraction fraction E is defined as:

$$E = 1 - e^{\frac{PS}{BF}}. \qquad (3)$$

Schematic representation of the Johnson–Wilson model, as well as the modifications due to St Lawrence and Lee, is presented in Figure 1. These distributed parameter models enable the separation of BF and E, thus allowing for the calculation of the PS area product. The Johnson–Wilson model achieves this by modeling convection along the vessel as a constant flow velocity.[24]

For the modified Johnson–Wilson model, Eqs (1) and (2) lead to the following for the tissue curve, $C_t(t)$:

$$C_t(t) = BV \cdot C_a(t) + K^{trans} \int_0^t C_a(u) e^{\frac{K^{trans}}{v_e}(t-u)} du \qquad (4)$$

where v_e is the volume of EES per unit volume of tissue and K^{trans} is the flow extraction product (BV·E). From the

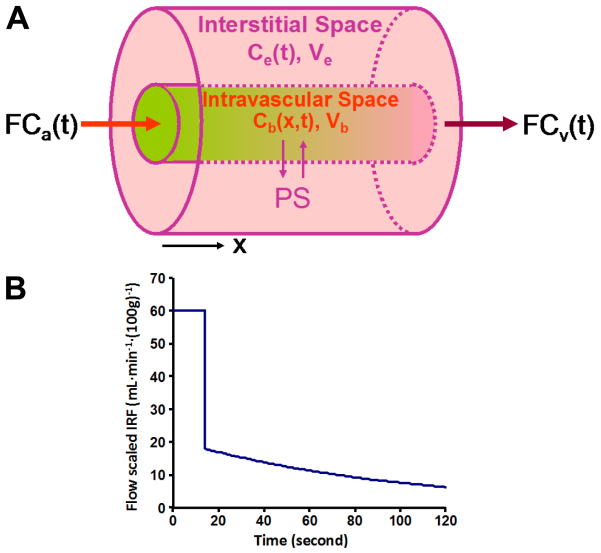

Figure 1. (**A**) Schematic drawing of the modified Johnson–Wilson model,[44] where the central cylinder represents all the vessels in the tissue region and the annulus around the cylinder is the interstitial space into or out of which contrast can diffuse. The interstitial space is assumed to be a *well-stirred* compartment, such that contrast concentration, $C_e(t)$ is uniformly distributed at any time. In the blood vessels, contrast concentration $C_b(x,t)$ changes with axial position (x) with respect to the arterial end as contrast diffuse into the interstitial space at a rate equal to the permeability surface product (PS). After the contrast bolus exits from the vessels, contrast in the interstitial space diffuses back into the vessels also at the rate of PS. F is the blood flow, $C_a(t)$ and $C_v(t)$ are the arterial and venous contrast concentrations, respectively, and V_b and V_e are the blood and interstitial volumes, respectively. (**B**) Flow-scaled impulse residue function [$R(t)$] of the modified Johnson–Wilson model for a tissue with BF, BF = 60 mL minute^{-1} (100 g^{-1}, V_b = 8.4 mL (100 g)$^{-1}$, vascular mean transit time 14 seconds, and PS = 21.4 mL minute^{-1} (100 g)$^{-1}$.

definition of E [Eq (3)], in the limit of PS = F, which is the case for brain tumors, K^{trans} ~ PS. A temporal resolution of 5–10 seconds per image is commonly used to balance the competing spatial resolution, scan coverage, and signal-to-noise ratio requirements when assessing permeability, but this acquisition rate is too slow for the measurements of BF and BV where a finer temporal resolution (1–2 seconds) is required.[41] While there is no consensus as to which CT acquisition technique is optimal for both perfusion and permeability quantitation,[46] acquisition techniques with different temporal resolutions, including initial high temporal resolution for perfusion measurement followed by lower temporal resolution acquisition for permeability measurement, are suggested to provide useful measurements and lowered radiation dose.[47]

Differences between CT- and MR-based DCE. While a similar analysis framework (ie, distributed parameter model) can be used to process DCE data acquired by CT or MR imaging, there are some notable differences between these modalities that need be discussed. First, the inherent image contrast mechanisms are different: CT DCE imaging measures contrast agent concentration, resulting from the changes in X-ray attenuation coefficient. MR DCE techniques measure the contrast agent concentration indirectly via the effect on the T1 relaxation rate on nearby water protons in the tissue. In MR DCE imaging, as previously described, additional kinetic modeling steps are required to convert from measured MR signal intensity to tracer concentration. CT contrast agent is iodine based,[48] while MR is gadolinium based.[39] Comparison of tumor parametric maps derived by DCE-CT and MR are reported to have consistent findings.[49] A close correlation of independently derived quantitative parameters from DCE-CT and MR indicates that both are measuring the same underlying tumor physiology.[49] Table 2 summarizes and compares the key aspects of DCE-MR and DCE-CT.

DCE-CT perfusion and permeability imaging—implementation details. DCE-CT refers to the acquisition of serial CT images to track the passage of a bolus of iodinated contrast agent. The typical DCE-CT protocol takes 2–3 minutes, and it involves rapid acquisition of images (1–2 seconds per image) during the initial phase of imaging (45 seconds) to capture the first pass of contrast agent for the calculation of BF and BV. To decrease the radiation dose, the second phase that involves less-frequent acquisition (10–15-second image interval) is required to calculate PS or K^{trans}.[24]

The clinical use of DCE-CT was initially slow to develop due to its relatively limited scan volume (2–4 cm coverage) and associated radiation dose (2–5 mSv).[40] Larger multirow detector technology now allows for the coverage of 16 cm of the anatomy.[50] Shuttle mode imaging can also increase the scan coverage.[51] More advanced reconstruction methods, such as adaptive statistical iterative reconstruction technique,[52] and reducing the temporal resolution of image acquisition (≤3 seconds) in the first phase[53] have both been demonstrated as effective ways to reduce the dose. Figure 2 shows an example for CT DCE perfusion and permeability images obtained in an anaplastic oligodendroglioma patient.

DCE-MR perfusion and permeability imaging—implementation details. DCE-MR refers to the acquisition of serial MR images using a T1-weighted sequence. The increase in T1 relaxation rate from the corresponding increases in contrast agent concentration results in an increase in MR signal intensity. DCE-MR scan duration is normally less than two minutes, but scans from three to six minutes are required if the rate of extravasation of contrast agent from the intravascular space into the EES (ie, PS or K^{trans}) is to be measured. Typically, the whole brain is acquired at a temporal acquisition rate of an image volume every two seconds. Recent techniques such as multichannel parallel imaging, multislice imaging, and compressed sensing can preserve whole-brain coverage and achieve finer temporal resolution.[54] Figure 3 provides an example for MR DCE perfusion and permeability images for a postresection GBM patient showing normal-appearing parenchyma and recurrent tumor.

Table 2. Comparison of MR and CT DCE techniques.

PARAMETER	MR DCE	CT DCE
Source of signal	Decrease in T1 of surrounding water molecules	Attenuation of x-ray by iodinated contrast
Change in signal intensity	Signal gain—assumed proportional to increasing contrast agent concentration	Signal gain—assumed proportional to increasing contrast agent concentration
Tracer kinetic analysis method	Compartmental model and distributed parameter models	Compartmental and distributed parameter models
Quantitative techniques	Relative and absolute	Relative and absolute
Typical Scan coverage	Close to whole brain	4 cm, 8 cm, and 16 cm coverage with multidetector CT system
Typical temporal resolution	5 s to 10 s	First phase: 1 s to 2 s Second phase: ≤5 s for Patlak model[43] and 10 s to 15 s for Johnson and Wilson model[44]
Typical scan duration, perfusion only	90 s	45 s
Typical scan duration, perfusion and permeability	5 min to 10 min	2 min to 3 min
Representative contrast agent	Gadopentetate dimeglumine	Iopamidol
Molecular weight of representative contrast agent	938 g/mol (0.938 kDa)	777 g/mol (0.777 kDa)

Applications of Perfusion and Permeability Biomarkers in Brain Cancer

Multiple applications for perfusion and permeability imaging of brain tumors have been explored to enhance the treatment planning process, to optimize treatment decision-making, to enable treatment monitoring, and to assess prognosis. In this section, we selectively target and review three key applications: differentiating malignant brain lesions, distinguishing true progression from posttreatment effects, and predicting survival after treatment therapies.

Differentiation of malignant brain lesions. Solitary brain metastases with no history of primary cancer are found in approximately 15% of patients and may have similar imaging features to primary malignant gliomas on conventional MR images.[55] Two factors should be considered when using perfusion imaging to differentiate solitary brain

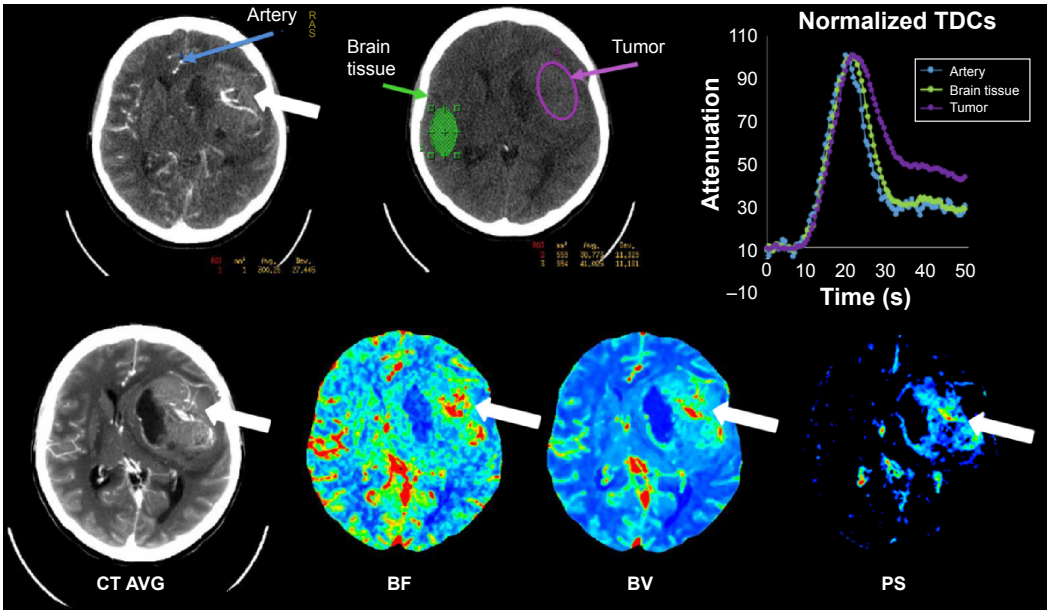

Figure 2. CT Perfusion technique in a patient with an anaplastic oligodendroglioma, prior to subtotal resection of the tumor. A series of images were acquired with contrast injection. In the top row of the figure, the artery region (blue line in the left panel), normal (green region in the central panel in the top row), and tumor (purple line in the central panel in top row) are shown in a CT image at peak enhancement and in a baseline CT image before contrast arrival. The corresponding background subtracted time–density curves (normalized to the same maximum) are also shown using the same color-coding scheme. In the bottom row of the figure, the time-averaged CT image, BF, BV, and PS maps in the same CT slice as in the top row are shown. White arrows point to the tumor in the different images and functional maps.

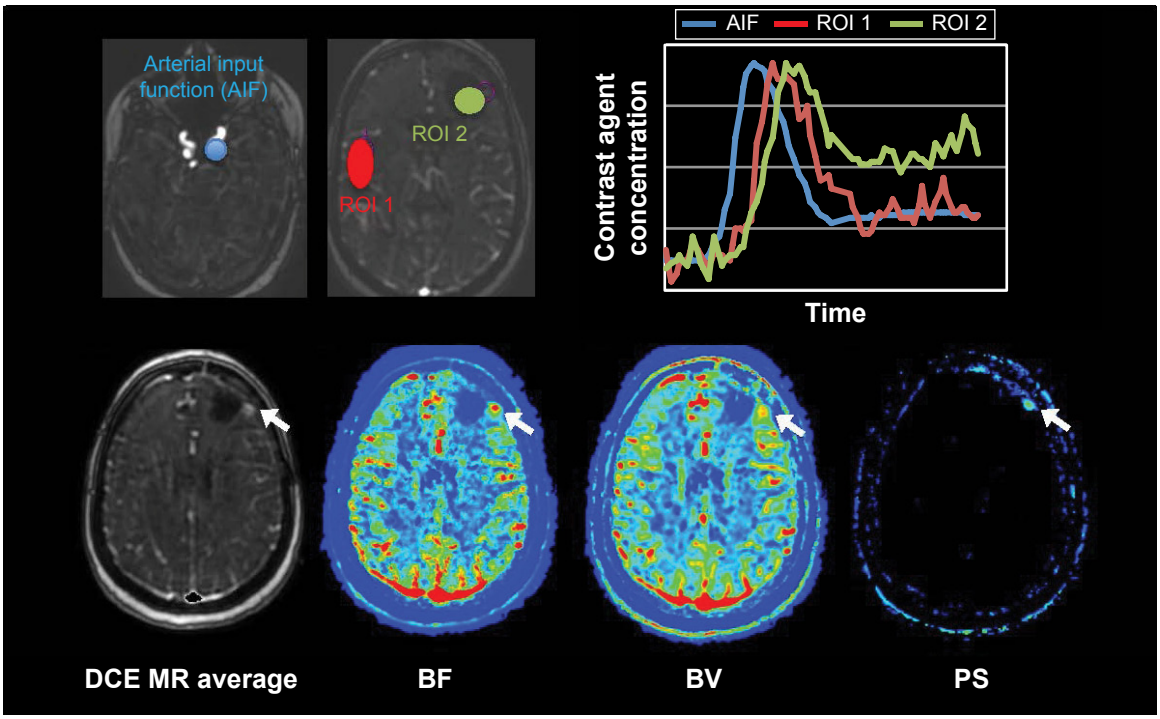

Figure 3. MR DCE technique in a GBM patient postresection. Analogous to CT DCE example (Fig. 2), a series of pre- and postcontrast agent injection images are acquired to measure contrast concentration over time (see text) in order to derive contrast agent vs time–concentration curves and parameter maps, such as cerebral BF, cerebral BV, and PS using the modified Johnson–Wilson model. White arrows point to the recurrent tumor.

metastases from malignant gliomas. First, current evidence suggests that BV in the contrast-enhancing metastatic lesion depends on the primary tumor site.[56] Metastases from melanoma and renal carcinoma, for example, are reported to have higher BV than malignant gliomas.[57] Studies that considered different sites of origin as one entity (or those that did not report primary tumor) showed that the BV of the enhancing metastatic lesions was either similar[58,59] or lower[60,61] than the malignant gliomas. Together, these studies suggest that the differentiation of brain metastasis from malignant glioma based on the BV of the contrast-enhancing lesion alone is challenging. Second, BV in the nonenhancing lesion shows promise for distinguishing metastases from primary malignant gliomas. For example, on CT or MR imaging, a low-intensity region (CT, T1 MR) or high-intensity lesion (T2 MR) around an enhancing lesion may represent edema or infiltrating tumor or a combination of both. In the case of metastases, infiltration more than 1–2 mm beyond the enhancing tumor is rare[62] so this region most often represents edema, while in malignant glioma, infiltration 1–2 cm is not uncommon. The high BV in the nonenhancing malignant glioma lesion can be attributed to their aggressive and infiltrative growth, which often extends into the surrounding T2-hyperintense region. The median sensitivity and specificity for distinguishing between nonenhancing lesions and gliomas using BV were 90% (range: 77%–100%) and 95% (64%–100%), respectively.[60,61,63] In contrast, the median sensitivity and specificity for contrast-enhancing lesions' vs gliomas' nBV (see definition in Table 1) were 87% (80%–91%) and 72% (64%–88%), respectively.[63,64]

Perfusion imaging can also differentiate malignant gliomas (Grades III and IV) from other primary brain tumors. These include differentiating primary malignant gliomas from lymphomas,[65,66] meningiomas,[67] hemangioblastomas,[67] and schwannomas.[67] Some studies have used perfusion imaging to differentiate subtypes of primary brain tumors.[68,69] Grade II and III oligodendroglial tumors showed higher nBV than both Grade II and III oligoastrocytic and astrocytic tumors, and oligoastrocytic tumors showed higher maximum nBV than astrocytic tumours.[70] A sensitivity and specificity of 100% and 88%, respectively, were found when nBV was used to differentiate Grade II and III oligodendroglial tumors from astrocytic tumors. Although there were differences in BV between the different types of primary brain tumors, the number of brain tumor types make this method of differentiation impractical.

Perfusion can help distinguish between high-and low-grade gliomas.[71] High-grade gliomas, particularly Grade IV, are highly infiltrative tumors with recurrence typically arising within 2 cm of the irradiated volume.[72] An active area of study is to evaluate the prognostic value of perfusion imaging for predicting the overall survival of patients with high-grade gliomas. An example of presurgery CT perfusion and MR images of two high-grade glioma patients is shown in Figure 4.

It is important to note that differentiation of tumor grade in oligodendroglial tumors based solely on perfusion imaging

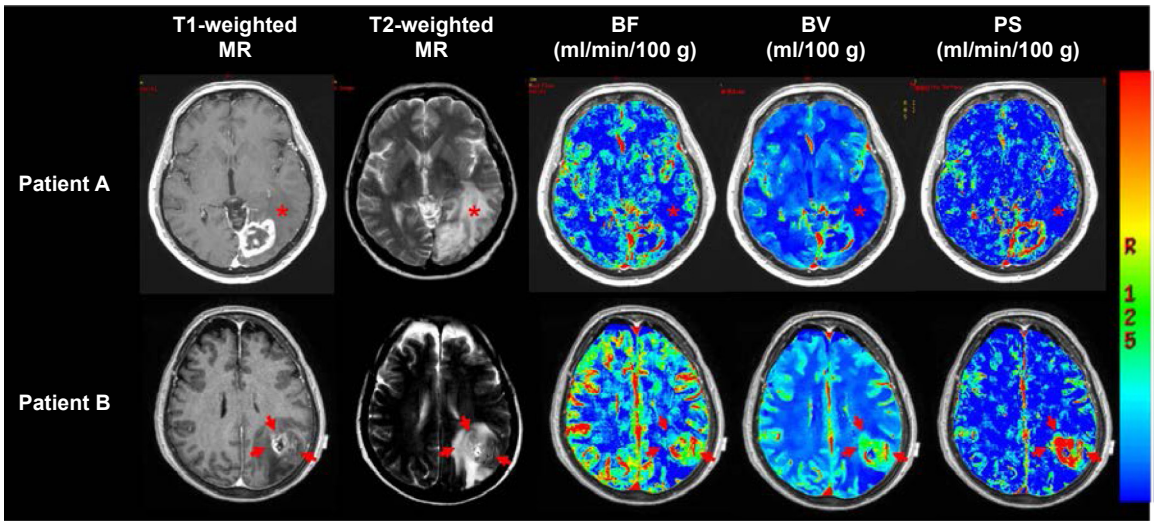

Figure 4. Illustrative presurgery CT perfusion and MR images of two patients both with Grade IV gliomas. Both patients presented with a contrast-enhancing lesion on postgadolinium T1-weighted MR images, which also had elevated BF, BV, and PS. Patient A presented with low BF, BV, and PS in the nonenhancing lesion (NEL, asterisk). Patient B presented with regions of elevated BF, BV, and PS in the NEL (red arrows). The survival for patient A was 41.6 months and patient B was 16.7 months. Color bar scale for maps is as follows: 10–75 mL minute^{-1} (100 g)$^{-1}$ for BF, 0.5–10 mL (100 g)$^{-1}$ for BV, and 1–10 mL minute^{-1} (100 g)$^{-1}$ for PS. This figure was reproduced from Ref. 98 with the permission of the copyright holder.

should be interpreted with some caution since there is evidence that oligodendroglial tumors can have higher BV than astrocytic tumors, irrespective of the tumor grade.[70] However, high-grade oligodendroglial tumors may or may not have higher BV than low-grade oligodendroglial tumors.[70,73] Therefore, perfusion imaging-based assessment of oligodendroglial tumors should be considered separately from astrocytic tumors, and perfusion imaging alone does not seem to provide a reliable criterion for differentiating oligodendroglial tumor grade.

Differentiation of progression from posttreatment effects. A change in the size of the contrast-enhancing tumor is used as a radiologic measure of progression, but it can be confounded by other sources of contrast enhancement. Pseudoprogression and treatment-induced necrosis (TIN) are posttreatment scenarios with a better prognosis than true progression, but their changes in contrast enhancement pattern can be indistinguishable from tumor progression.[74] Erroneous diagnosis of pseudoprogression or TIN as tumor progression can lead to unnecessary treatment or premature abandonment of treatment. Interpreting progression incorrectly may delay the treatment.

Pseudoprogression occurs in 20%–30% of malignant glioma patients treated with chemoirradiation and manifests as a transient increase in tumor contrast enhancement at one to three months posttreatment that eventually subsides.[75,76] Although its pathophysiology remains unclear, chemoirradiation is believed to induce a transient local inflammatory reaction, edema, and increased vessel permeability, which manifests as increased signal on contrast-enhanced images.[77] Also, radiation injury can induce an increase of VEGF, which can subsequently lead to perfusion increase. However, there is evidence that when using DSC MR perfusion imaging, true progression had a higher maximum nBV than pseudoprogression when confirmed by radiologic and clinical follow-ups (sensitivity and specificity of 81.5% and 77.8%, respectively).[76,78] Another study showed that both nBV and nPH could distinguish pseudoprogression from progression with sensitivities and specificities of both ≥75%.[79] Histogram analysis of nBV to characterize percent changes in nBV skewness and kurtosis is also a potential biomarker for differentiating pseudoprogression from true progression.[80] In another prospective study, a decrease in nBV after three weeks of chemoirradiation was associated with a higher risk of early progression.[75] Also, TIN occurs 3–12 months after radiotherapy in 3%–24% of patients.[77] Radiation-induced necrosis and pseudoprogression were collectively defined as radiation-induced injury in eight MR perfusion studies.[81] Mean and maximum nBV were reported to differentiate radiation-induced injury from true progression with sensitivities and specificities ranging from 86% to 100% and 80% to 100%, respectively.[82,83] Radiation-induced injury and true progression often coexist in patients. Hu et al showed that MR perfusion imaging was able to estimate the fractional tumor burden (ie, progression) and posttreatment effect (ie, radiation-induced injury) within the same MR contrast-enhancing lesion.[84] This fractional tumor burden strongly correlated with the histological tumor fraction obtained from stereotactic biopsy ($r = 0.82$, $P < 0.001$) and correlated with the overall survival ($P < 0.02$). These results demonstrate that MR may be a useful clinical tool to differentiate progression from posttreatment effects.

Survival after radiotherapy and chemotherapy. The value of perfusion imaging in predicting progression-free

survival (PFS) and overall survival has been investigated in numerous studies. The interpretation of perfusion imaging data for predictive survival depends on treatment regimen and imaging schedule. Three perfusion imaging schedules for predicting outcomes have been reported as follows: (1) pretreatment, (2) pretreatment and midtreatment, and (3) pretreatment and posttreatment. Figure 5 shows an example of perfusion and permeability surface maps at preradiotherapy, near-end-of-radiotherapy, and with tumor progression.

When pre-chemoirradiation MR perfusion images were considered, a higher mean and maximum nBV were associated with poor PFS and lower overall survival for gliomas of all grades.[85–87] The two-year overall survival rate for Grade III astrocytomas was significantly lower for patients with maximum nBV > 2.3 (33% vs 100%, $P < 0.01$), and it was also lower for GBM (5% vs 25%, $P = 0.013$).[85] Using DCE-CT imaging, a combination of high BV and PS was associated with poor overall survival for Grade III and IV gliomas and for Grade IV gliomas alone.[88,89] In patients with GBM, k_{ep} values ≤ 1.2 minute^{-1}, between 1.21 and 2.0 minute^{-1}, and >2.0 minute^{-1} had one-year overall survival rate of 59%, 33%, and 15%, respectively (P value not reported).[90] These studies suggest that pretreatment higher BV, higher PS, and higher k_{ep} were associated with more aggressive phenotypes that conferred poor survival.

The prognostic value of comparing pre- and midradiotherapy perfusion imaging parameters has been investigated.[91,92] Based on the parametric response map analysis, a decrease in tumor BV and BF at one and three weeks into chemoirradiation were predictive of poor overall survival.[91,92] Specifically, patients with >6.8% of tumor volume, showing a decrease in nBV, had reduced overall survival than those with ≤6.8% of tumor volume, showing a decrease in nBV (median overall survival of 7.1 and 20.4 months, respectively; $P = 0.001$).[91] A drop in BV during treatment suggests increased tumor hypoxia, leading to chemoirradiation resistance. These studies suggest that BF and BV measurements can potentially identify the patients with poor survival even before the completion of chemoirradiation.

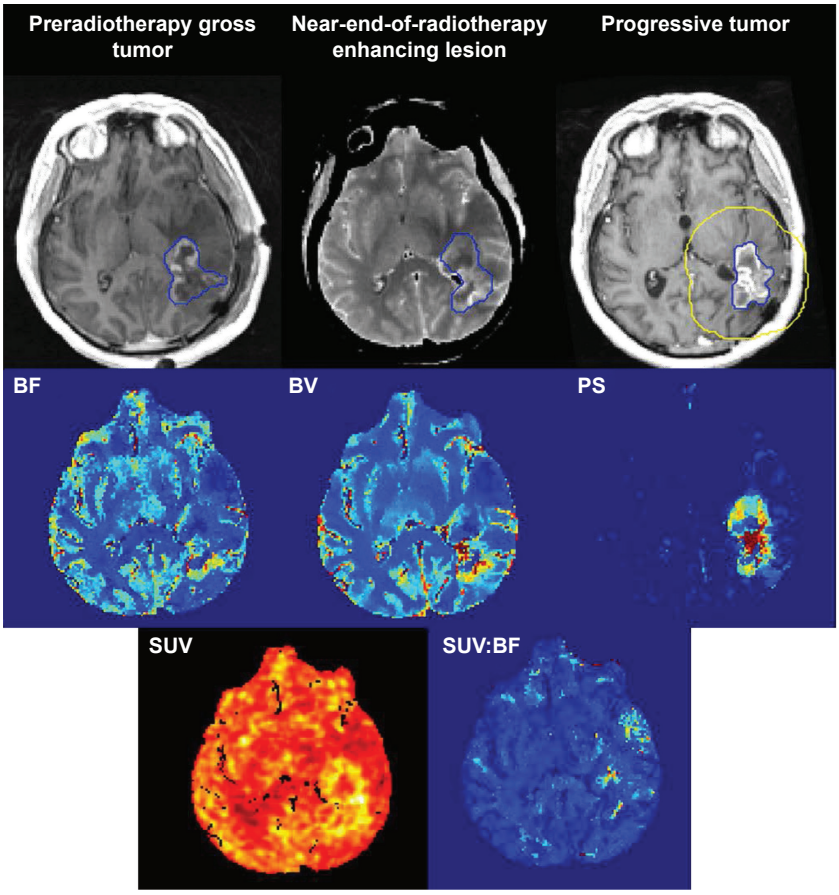

Figure 5. Preradiotherapy gross tumor (T1-weighted MR), near-end-of radiotherapy enhancing lesion (averaged CT), and progressive tumor (T1-weighted MR); and the corresponding parametric maps of BF, BV, PS, standard uptake value (SUV), and SUV:BF ratio acquired using CT perfusion and FDG-PET. Blue outlines show the contrast-enhancing lesions delineated by a radiation oncologist. Yellow outline is the 2 cm bounding box that was set for performing analysis of neighboring pixels. This figure originally appeared in the *Journal of Medical Radiation Sciences*, 2014;61:4–13 and was reproduced under terms of the Creative Commons Attribution License with the permission of the copyright holder.[110]
Abbreviations: MR, magnetic resonance; CT, computed tomography; FDG-PET, 18-fluorodeoxyglucose positron emission tomography.

Tumor perfusion after the completion of chemoirradiation and its association with survival have also been investigated.[93,94] An increase in the maximum nBF between baseline and follow-up imaging was a better prognosticator of shorter PFS (hazard ratio [HR] = 2.67, $P = 0.010$) than an increase in tumor diameter (HR = 1.14, $P = 0.049$).[95] At one-month postradiotherapy, Mangla et al showed that an increase in nBV was predictive of poor one-year overall survival (sensitivity = 90% and specificity = 69%), while the tumor size was not.[96] However, another study showed that perfusion imaging was not predictive of survival, while tumor diameters by T1- and T2-weighted imaging were predictive.[93] Using ferumoxytol (an iron-based MR contrast agent) postradiotherapy, lower tumor nBV predicted patients with longer overall survival ($P < 0.001$).[97] In the nonenhancing lesion, Li et al showed that a higher median nBV immediately after radiation was associated with shorter PFS ($P = 0.026$).[94] Finally, Yeung et al[98] showed higher trends in BF, BV, and PS in the contrast-enhancing lesions and the nonenhancing lesions in patients with OS < 18 months compared with those with OS ≥ 18 months.

In summary, a high BV before and after chemoirradiation and a decrease in BV during chemoirradiation are associated with poor survival. A high BV before and after treatment is characteristic of tumor growth and progression, while a decrease in BV during treatment may be indicative of tumor hypoxia.

Survival after antiangiogenic therapy. Radiologic assessment of response to antiangiogenic agents, especially those that target VEGF, should be interpreted with caution because a decrease in contrast enhancement is not necessarily indicative of true response (ie, it may be a pseudoresponse).[26] Batchelor et al[99] showed that patients treated with cediranib demonstrated decreased MR signal enhancement as early as one day after the initiation of treatment, despite considerable variability in tumor response. Given the vascular effects of antiangiogenic agents, DCE perfusion imaging may potentially play an important role in providing insight and assessing response to these agents.

For recurrent GBMs, high nBV and K^{trans} prior to anti-VEGF monotherapy or in combination with temozolomide were associated with poor survival. Tumor BF,[99] nBV,[99,100] K^{trans},[101] and v_e[102] decreased shortly after the initiation of bevacizumab or cediranib. In the nonenhancing lesions, nBV could also decrease after bevacizumab treatment, suggesting that the drug may have an antiedema effect (statistical significance not reported).[103] There is no consensus on whether a decrease in these parameters is a positive prognosticator. A decrease in K^{trans} and nBV after bevacizumab treatment did not show a significant association with PFS or overall survival in some studies.[104] In another study, a decrease in tumor subvolume with nBV > 1.00 after bevacizumab treatment was associated with longer time to progression.[105] A reduction in K^{trans} after cediranib treatment was associated with improved PFS and OS.[106] A moderate correlation (Spearman's $\rho = 0.58$, $P = 0.036$) between overall survival and K^{trans} at one week after stereotactic radiosurgery and bevacizumab was reported in patients with recurrent malignant gliomas.[107]

The inconsistent relationships found between various perfusion and permeability imaging parameters and overall survival suggest that not all patients responded equally to antiangiogenic agents. Sorensen et al showed that 25% of patients with recurrent GBMs treated with cediranib exhibited elevated perfusion, and these patients had higher PFS and overall survival than those with stable or decreased perfusion.[106] This finding was confirmed in patients with newly diagnosed gliblastomas that were treated with radiotherapy, temozolomide, and cediranib. Patients with increased perfusion had a significantly longer median overall survival than patients with decreased perfusion (overall survival of 504 vs 321 days; log-rank $P < 0.05$).[103] Increased perfusion was also associated with improved tumor oxygenation, which could potentially improve the sensitization of tumor cells to chemoirradiation and enhance the delivery of temozolomide to the tumor. In a study involving patients with recurrent malignant gliomas, independent component analysis of MR perfusion images was used to characterize the extent of abnormal vasculature before and after bevacizumab treatment. A decrease in the arteriovenous overlap (ie, a decrease of abnormal vasculature) was associated with longer overall survival in these patients ($P < 0.04$), whereas a change in the tumor volume and nBV was not predictive of overall survival.[108] In aggregate, these results suggest that perfusion imaging may be a tool for selecting the appropriate patients for antiangiogenic therapies. More prospective information preferably gathered at multiple centers with high quality control is needed to clarify the reported heterogeneities in results.[109]

Summary

We provided an overview of DCE-CT and MR perfusion and permeability principles, parameters, and applications in brain cancer. These perfusion and permeability quantification approaches may serve as potential biomarkers for differentiation of malignant lesions and posttreatment effects and for investigations on survival after radiotherapy, chemotherapy, and antiangiogenic treatments.

Abbreviations

ASL, arterial spin labeling; BBB, blood–brain barrier; BF, blood flow; BV, blood volume; CT, computed tomography; DCE, dynamic contrast-enhancement; DSC, dynamic susceptibility contrast; EES, extravascular extracellular space; GBM, glioblastoma; HR, hazard ratio; MR, magnetic resonance; nBF, normalized blood flow; nBV, normalized blood volume; PFS, progression-free survival; PS, permeability surface area product; RANO, response assessment in neuro-oncology; TIN, treatment-induced necrosis; WHO, World Health Organization.

Acknowledgments

We would like to acknowledge the support of the Canadian Institutes for Health Research (CIHR); the Medical Imaging Trials Network of Canada (MITNEC) was funded by the CIHR. TYL and RF are investigators with MITNEC. AE was University of Calgary Eye's high postdoctoral scholar. CDD was a Heart and Stroke Foundation of Canada Fellow. AE and CDD were also supported by the International and Industrial Imaging Training (I3T) program funded by the Natural Science and Engineering Research Council of Canada Collaborative Research and Training Experience (NSERC CREATE) program. RF is the Hopewell Professor of Brain Imaging.

Author Contributions

Wrote the first draft of the manuscript: AE. Contributed to the writing of the manuscript: AE, TY, CE, GB, SY, JE, EF, TYL, and RF. Agree with manuscript results and conclusions: AE, TY, CE, GB, SY, JE, EF, TYL, and RF. Jointly developed the structure and arguments for the paper: AE, TYL, RF. Made critical revisions and approved final version: AE, TY, CE, GB, SY, JE, EF, TYL, and RF. All authors reviewed and approved of the final manuscript.

REFERENCES

1. Ostrom QT, Gittleman H, Liao P, et al. CBTRUS statistical report: primary brain and central nervous system tumors diagnosed in the United States in 2007–2011. *Neuro Oncol*. 2014;16(suppl 4):iv1–iv63.
2. Siegel R, Ma J, Zou Z, Jemal A. Cancer statistics, 2014. *CA Cancer J Clin*. 2014;64:9–29.
3. Liu R, Page M, Solheim K, Fox S, Chang SM. Quality of life in adults with brain tumors: current knowledge and future directions. *Neuro Oncol*. 2009;11:330–339.
4. Louis DN, Ohgaki H, Wiestler OD, et al. The 2007 WHO classification of tumours of the central nervous system. *Acta Neuropathol*. 2007;114:97–109.
5. Fuller GN, Scheithauer BW. The 2007 Revised World Health Organization (WHO) Classification of Tumours of the Central Nervous System: newly codified entities. *Brain Pathol*. 2007;17:304–307.
6. Stupp R, Mason WP, van den Bent MJ, et al; European Organisation for Research and Treatment of Cancer Brain Tumor and Radiotherapy Groups; National Cancer Institute of Canada Clinical Trials Group. Radiotherapy plus concomitant and adjuvant temozolomide for glioblastoma. *N Engl J Med*. 2005;352:987–996.
7. McGirt MJ, Chaichana KL, Gathinji M, et al. Independent association of extent of resection with survival in patients with malignant brain astrocytoma. *J Neurosurg*. 2009;110:156–162.
8. Chan JL, Lee SW, Fraass BA, et al. Survival and failure patterns of high-grade gliomas after three-dimensional conformal radiotherapy. *J Clin Oncol*. 2002;20:1635–1642.
9. Narayana A, Yamada J, Berry S, et al. Intensity-modulated radiotherapy in high-grade gliomas: clinical and dosimetric results. *Int J Radiat Oncol Biol Phys*. 2006;64:892–897.
10. Coffey RJ, Lunsford LD, Taylor FH. Survival after stereotactic biopsy of malignant gliomas. *Neurosurgery*. 1988;22:465–473.
11. Thompson G, Mills SJ, Coope DJ, O'Connor JP, Jackson A. Imaging biomarkers of angiogenesis and the microvascular environment in cerebral tumours. *Br J Radiol*. 2011;84(Spec No 2):S127–S144.
12. Jakubovic R, Sahgal A, Soliman H, et al. Magnetic resonance imaging-based tumour perfusion parameters are biomarkers predicting response after radiation to brain metastases. *Clin Oncol (R Coll Radiol)*. 2014;26:704–712.
13. Padhani AR. MRI for assessing antivascular cancer treatments. *Br J Radiol*. 2003;76(Spec No 1):S60–S80.
14. Liebner S, Fischmann A, Rascher G, et al. Claudin-1 and claudin-5 expression and tight junction morphology are altered in blood vessels of human glioblastoma multiforme. *Acta Neuropathol*. 2000;100:323–331.
15. Barlow KD, Sanders AM, Soker S, Ergun S, Metheny-Barlow LJ. Pericytes on the tumor vasculature: jekyll or hyde? *Cancer Microenviron*. 2013;6:1–17.
16. Janzer RC, Raff MC. Astrocytes induce blood–brain barrier properties in endothelial cells. *Nature*. 1987;325:253–257.
17. Lamszus K, Laterra J, Westphal M, Rosen EM. Scatter factor/hepatocyte growth factor (sf/hgf) content and function in human gliomas. *Int J Dev Neurosci*. 1999;17:517–530.
18. Raghunand N, Gatenby RA, Gillies RJ. Microenvironmental and cellular consequences of altered blood flow in tumours. *Br J Radiol*. 2003;76(Spec No 1):S11–S22.
19. Rijken PF, Bernsen HJ, Peters JP, Hodgkiss RJ, Raleigh JA, van der Kogel AJ. Spatial relationship between hypoxia and the (perfused) vascular network in a human glioma xenograft: a quantitative multi-parameter analysis. *Int J Radiat Oncol Biol Phys*. 2000;48:571–582.
20. Hardee ME, Zagzag D. Mechanisms of glioma-associated neovascularization. *Am J Pathol*. 2012;181:1126–1141.
21. Price SJ, Gillard JH. Imaging biomarkers of brain tumour margin and tumour invasion. *Br J Radiol*. 2011;84(Spec No 2):S159–S167.
22. Payne GS, Leach MO. Applications of magnetic resonance spectroscopy in radiotherapy treatment planning. *Br J Radiol*. 2006;79(Spec No 1):S16–S26.
23. Macdonald DR, Cascino TL, Schold SC Jr, Cairncross JG. Response criteria for phase II studies of supratentorial malignant glioma. *J Clin Oncol*. 1990;8:1277–1280.
24. Lee TY, Purdie TG, Stewart E. CT imaging of angiogenesis. *Q J Nucl Med*. 2003;47:171–187.
25. Meier P, Zierler KL. On the theory of the indicator-dilution method for measurement of blood flow and volume. *J Appl Physiol*. 1954;6:731–744.
26. Wen PY, Macdonald DR, Reardon DA, et al. Updated response assessment criteria for high-grade gliomas: response assessment in neuro-oncology working group. *J Clin Oncol*. 2010;28:1963–1972.
27. Griffith B, Jain R. Perfusion imaging in neuro-oncology: basic techniques and clinical applications. *Radiol Clin North Am*. 2015;53:497–511.
28. Qiao XJ, Ellingson BM, Kim HJ, et al. Arterial spin-labeling perfusion MRI stratifies progression-free survival and correlates with epidermal growth factor receptor status in glioblastoma. *AJNR Am J Neuroradiol*. 2015;36:672–677.
29. Silva AC, Kim SG, Garwood M. Imaging blood flow in brain tumors using arterial spin labeling. *Magn Reson Med*. 2000;44:169–173.
30. Pollock JM, Tan H, Kraft RA, Whitlow CT, Burdette JH, Maldjian JA. Arterial spin-labeled MR perfusion imaging: clinical applications. *Magn Reson Imaging Clin N Am*. 2009;17:315–338.
31. Alsop DC, Detre JA, Golay X, et al. Recommended implementation of arterial spin-labeled perfusion MRI for clinical applications: a consensus of the ISMRM perfusion study group and the European consortium for ASL in dementia. *Magn Reson Med*. 2015;73(1):102–116.
32. Ostergaard L. Cerebral perfusion imaging by bolus tracking. *Top Magn Reson Imaging*. 2004;15:3–9.
33. Ostergaard L. Principles of cerebral perfusion imaging by bolus tracking. *J Magn Reson Imaging*. 2005;22:710–717.
34. Chen JJ, Smith MR, Frayne R. Advantages of frequency-domain modeling in dynamic-susceptibility contrast magnetic resonance cerebral blood flow quantification. *Magn Reson Med*. 2005;53:700–707.
35. Chen JJ, Smith MR, Frayne R. The impact of partial-volume effects in dynamic susceptibility contrast magnetic resonance perfusion imaging. *J Magn Reson Imaging*. 2005;22:390–399.
36. Paulson ES, Schmainda KM. Comparison of dynamic susceptibility-weighted contrast-enhanced MR methods: recommendations for measuring relative cerebral blood volume in brain tumors. *Radiology*. 2008;249:601–613.
37. Wu S, Thornhill RE, Chen S, Rammo W, Mikulis DJ, Kassner A. Relative recirculation: a fast, model-free surrogate for the measurement of blood-brain barrier permeability and the prediction of hemorrhagic transformation in acute ischemic stroke. *Invest Radiol*. 2009;44:662–668.
38. Sourbron SP, Buckley DL. Tracer kinetic modelling in MRI: estimating perfusion and capillary permeability. *Phys Med Biol*. 2012;57:R1–R33.
39. MacDonald ME, Frayne R. Cerebrovascular MRI: a review of state-of-the-art approaches, methods and techniques. *NMR Biomed*. 2015;28(7):767–791.
40. Yeung TP, Yartsev S, Bauman G, He W, Fainardi E, Lee TY. The effect of scan duration on the measurement of perfusion parameters in CT perfusion studies of brain tumors. *Acad Radiol*. 2013;20:59–65.
41. Ingrisch M, Dietrich O, Attenberger UI, et al. Quantitative pulmonary perfusion magnetic resonance imaging: influence of temporal resolution and signal-to-noise ratio. *Invest Radiol*. 2010;45:7–14.
42. Tofts PS, Brix G, Buckley DL, et al. Estimating kinetic parameters from dynamic contrast-enhanced t(1)-weighted MRI of a diffusable tracer: standardized quantities and symbols. *J Magn Reson Imaging*. 1999;10:223–232.
43. Patlak CS, Blasberg RG, Fenstermacher JD. Graphical evaluation of blood-to-brain transfer constants from multiple-time uptake data. *J Cereb Blood Flow Metab*. 1983;3:1–7.
44. Johnson JA, Wilson TA. A model for capillary exchange. *Am J Physiol*. 1966;210:1299–1303.

45. St Lawrence KS, Lee TY. An adiabatic approximation to the tissue homogeneity model for water exchange in the brain: II. Experimental validation. *J Cereb Blood Flow Metab*. 1998;18:1378–1385.
46. O'Connor JP, Tofts PS, Miles KA, Parkes LM, Thompson G, Jackson A. Dynamic contrast-enhanced imaging techniques: CT and MRI. *Br J Radiol*. 2011;84(Spec No 2):S112–S120.
47. Miles KA. Perfusion CT for the assessment of tumour vascularity: which protocol? *Br J Radiol*. 2003;76(Spec No 1):S36–S42.
48. Yeung TP, Bauman G, Yartsev S, Fainardi E, Macdonald D, Lee TY. Dynamic perfusion CT in brain tumors. *Eur J Radiol*. 2015;84(12):2386–2392.
49. Yang C, Stadler WM, Karczmar GS, Milosevic M, Yeung I, Haider MA. Comparison of quantitative parameters in cervix cancer measured by dynamic contrast-enhanced MRI and CT. *Magn Reson Med*. 2010;63:1601–1609.
50. Coolens C, Breen S, Purdie TG, et al. Implementation and characterization of a 320-slice volumetric CT scanner for simulation in radiation oncology. *Med Phys*. 2009;36:5120–5127.
51. Youn SW, Kim JH, Weon YC, Kim SH, Han MK, Bae HJ. Perfusion CT of the brain using 40-mm-wide detector and toggling table technique for initial imaging of acute stroke. *AJR Am J Roentgenol*. 2008;191:W120–W126.
52. Prakash P, Kalra MK, Kambadakone AK, et al. Reducing abdominal CT radiation dose with adaptive statistical iterative reconstruction technique. *Invest Radiol*. 2010;45:202–210.
53. Wiesmann M, Berg S, Bohner G, et al. Dose reduction in dynamic perfusion CT of the brain: effects of the scan frequency on measurements of cerebral blood flow, cerebral blood volume, and mean transit time. *Eur Radiol*. 2008;18:2967–2974.
54. Essig M, Shiroishi MS, Nguyen TB, et al. Perfusion MRI: the five most frequently asked technical questions. *AJR Am J Roentgenol*. 2013;200:24–34.
55. Schiff D. Single brain metastasis. *Curr Treat Options Neurol*. 2001;3:89–99.
56. Fan GG, Deng QL, Wu ZH, Guo QY. Usefulness of diffusion/perfusion-weighted MRI in patients with non-enhancing supratentorial brain gliomas: a valuable tool to predict tumour grading? *Br J Radiol*. 2006;79:652–658.
57. Kremer S, Grand S, Berger F, et al. Dynamic contrast-enhanced MRI: differentiating melanoma and renal carcinoma metastases from high-grade astrocytomas and other metastases. *Neuroradiology*. 2003;45:44–49.
58. Law M, Cha S, Knopp EA, Johnson G, Arnett J, Litt AW. High-grade gliomas and solitary metastases: differentiation by using perfusion and proton spectroscopic MR imaging. *Radiology*. 2002;222:715–721.
59. Ludemann L, Grieger W, Wurm R, Wust P, Zimmer C. Quantitative measurement of leakage volume and permeability in gliomas, meningiomas and brain metastases with dynamic contrast-enhanced MRI. *Magn Reson Imaging*. 2005;23:833–841.
60. Young GS, Setayesh K. Spin-echo echo-planar perfusion MR imaging in the differential diagnosis of solitary enhancing brain lesions: distinguishing solitary metastases from primary glioma. *AJNR Am J Neuroradiol*. 2009;30:575–577.
61. Mouthuy N, Cosnard G, Abarca-Quinones J, Michoux N. Multiparametric magnetic resonance imaging to differentiate high-grade gliomas and brain metastases. *J Neuroradiol*. 2012;39:301–307.
62. Baumert BG, Rutten I, Dehing-Oberije C, et al. A pathology-based substrate for target definition in radiosurgery of brain metastases. *Int J Radiat Oncol Biol Phys*. 2006;66:187–194.
63. Bulakbasi N, Kocaoglu M, Farzaliyev A, Tayfun C, Ucoz T, Somuncu I. Assessment of diagnostic accuracy of perfusion MR imaging in primary and metastatic solitary malignant brain tumors. *AJNR Am J Neuroradiol*. 2005;26:2187–2199.
64. Hakyemez B, Erdogan C, Gokalp G, Dusak A, Parlak M. Solitary metastases and high-grade gliomas: radiological differentiation by morphometric analysis and perfusion-weighted MRI. *Clin Radiol*. 2010;65:15–20.
65. Bendini M, Marton E, Feletti A, et al. Primary and metastatic intraaxial brain tumors: prospective comparison of multivoxel 2D chemical-shift imaging (CSI) proton MR spectroscopy, perfusion MRI, and histopathological findings in a group of 159 patients. *Acta Neurochir (Wien)*. 2011;153:403–412.
66. Weber MA, Zoubaa S, Schlieter M, et al. Diagnostic performance of spectroscopic and perfusion MRI for distinction of brain tumors. *Neurology*. 2006;66:1899–1906.
67. Hakyemez B, Yildirim N, Erdogan C, Kocaeli H, Korfali E, Parlak M. Meningiomas with conventional MRI findings resembling intraaxial tumors: can perfusion-weighted MRI be helpful in differentiation? *Neuroradiology*. 2006;48:695–702.
68. Narang J, Jain R, Scarpace L, et al. Tumor vascular leakiness and blood volume estimates in oligodendrogliomas using perfusion CT: an analysis of perfusion parameters helping further characterize genetic subtypes as well as differentiate from astroglial tumors. *J Neurooncol*. 2011;102:287–293.
69. Eliat PA, Olivie D, Saikali S, Carsin B, Saint-Jalmes H, de Certaines JD. Can dynamic contrast-enhanced magnetic resonance imaging combined with texture analysis differentiate malignant glioneuronal tumors from other glioblastoma? *Neurol Res Int*. 2012;2012:195176.
70. Saito T, Yamasaki F, Kajiwara Y, et al. Role of perfusion-weighted imaging at 3t in the histopathological differentiation between astrocytic and oligodendroglial tumors. *Eur J Radiol*. 2012;81:1863–1869.
71. Fainardi E, Di Biase F, Borrelli M, et al. Potential role of CT perfusion parameters in the identification of solitary intra-axial brain tumor grading. *Acta Neurochir Suppl*. 2010;106:283–287.
72. Weber DC, Casanova N, Zilli T, et al. Recurrence pattern after [(18)f] fluoroethyltyrosine-positron emission tomography-guided radiotherapy for high-grade glioma: a prospective study. *Radiother Oncol*. 2009;93:586–592.
73. Whitmore RG, Krejza J, Kapoor GS, et al. Prediction of oligodendroglial tumor subtype and grade using perfusion weighted magnetic resonance imaging. *J Neurosurg*. 2007;107:600–609.
74. Sharpton SR, Oermann EK, Moore DT, et al. The volumetric response of brain metastases after stereotactic radiosurgery and its post-treatment implications. *Neurosurgery*. 2014;74:9-15; discussion 16; quiz 16.
75. Tsien C, Galban CJ, Chenevert TL, et al. Parametric response map as an imaging biomarker to distinguish progression from pseudoprogression in high-grade glioma. *J Clin Oncol*. 2010;28:2293–2299.
76. Kong DS, Kim ST, Kim EH, et al. Diagnostic dilemma of pseudoprogression in the treatment of newly diagnosed glioblastomas: the role of assessing relative cerebral blood flow volume and oxygen-6-methylguanine-DNA methyltransferase promoter methylation status. *AJNR Am J Neuroradiol*. 2011;32:382–387.
77. Brandsma D, Stalpers L, Taal W, Sminia P, van den Bent MJ. Clinical features, mechanisms, and management of pseudoprogression in malignant gliomas. *Lancet Oncol*. 2008;9:453–461.
78. Gahramanov S, Raslan AM, Muldoon LL, et al. Potential for differentiation of pseudoprogression from true tumor progression with dynamic susceptibility-weighted contrast-enhanced magnetic resonance imaging using ferumoxytol vs. Gadoteridol: a pilot study. *Int J Radiat Oncol Biol Phys*. 2011;79:514–523.
79. Young RJ, Gupta A, Shah AD, et al. MRI perfusion in determining pseudoprogression in patients with glioblastoma. *Clin Imaging*. 2013;37:41–49.
80. Baek HJ, Kim HS, Kim N, Choi YJ, Kim YJ. Percent change of perfusion skewness and kurtosis: a potential imaging biomarker for early treatment response in patients with newly diagnosed glioblastomas. *Radiology*. 2012;264:834–843.
81. Kim HS, Kim JH, Kim SH, Cho KG, Kim SY. Posttreatment high-grade glioma: usefulness of peak height position with semiquantitative MR perfusion histogram analysis in an entire contrast-enhanced lesion for predicting volume fraction of recurrence. *Radiology*. 2010;256:906–915.
82. Fink JR, Carr RB, Matsusue E, et al. Comparison of 3 tesla proton MR spectroscopy, MR perfusion and MR diffusion for distinguishing glioma recurrence from posttreatment effects. *J Magn Reson Imaging*. 2012;35:56–63.
83. Bobek-Billewicz B, Stasik-Pres G, Majchrzak H, Zarudzki L. Differentiation between brain tumor recurrence and radiation injury using perfusion, diffusion-weighted imaging and MR spectroscopy. *Folia Neuropathol*. 2010;48:81–92.
84. Hu LS, Eschbacher JM, Heiserman JE, et al. Reevaluating the imaging definition of tumor progression: perfusion MRI quantifies recurrent glioblastoma tumor fraction, pseudoprogression, and radiation necrosis to predict survival. *Neuro Oncol*. 2012;14:919–930.
85. Hirai T, Murakami R, Nakamura H, et al. Prognostic value of perfusion MR imaging of high-grade astrocytomas: long-term follow-up study. *AJNR Am J Neuroradiol*. 2008;29:1505–1510.
86. Jenkinson MD, Smith TS, Joyce KA, et al. Cerebral blood volume, genotype and chemosensitivity in oligodendroglial tumours. *Neuroradiology*. 2006;48:703–713.
87. Jiang Z, Le Bas JF, Grand S, et al. Prognostic value of perfusion MR imaging in patients with oligodendroglioma: a survival study. *J Neuroradiol*. 2011;38:53–61.
88. Shankar JJ, Woulfe J, Silva VD, Nguyen TB. Evaluation of perfusion CT in grading and prognostication of high-grade gliomas at diagnosis: a pilot study. *AJR Am J Roentgenol*. 2013;200:W504–W509.
89. Jain R, Narang J, Griffith B, et al. Prognostic vascular imaging biomarkers in high-grade gliomas: tumor permeability as an adjunct to blood volume estimates. *Acad Radiol*. 2013;20:478–485.
90. Awasthi R, Pandey CM, Sahoo P, et al. Dynamic contrast-enhanced magnetic resonance imaging-derived kep as a potential biomarker of matrix metalloproteinase 9 expression in patients with glioblastoma multiforme: a pilot study. *J Comput Assist Tomogr*. 2012;36:125–130.
91. Galban CJ, Chenevert TL, Meyer CR, et al. Prospective analysis of parametric response map-derived MRI biomarkers: identification of early and distinct glioma response patterns not predicted by standard radiographic assessment. *Clin Cancer Res*. 2011;17:4751–4760.
92. Galban CJ, Chenevert TL, Meyer CR, et al. The parametric response map is an imaging biomarker for early cancer treatment outcome. *Nat Med*. 2009;15:572–576.
93. Leimgruber A, Ostermann S, Yeon EJ, et al. Perfusion and diffusion MRI of glioblastoma progression in a four-year prospective temozolomide clinical trial. *Int J Radiat Oncol Biol Phys*. 2006;64:869–875.
94. Li Y, Lupo JM, Polley MY, et al. Serial analysis of imaging parameters in patients with newly diagnosed glioblastoma multiforme. *Neuro Oncol*. 2011;13:546–557.
95. Voglein J, Tuttenberg J, Weimer M, et al. Treatment monitoring in gliomas: comparison of dynamic susceptibility-weighted contrast-enhanced and spectroscopic MRI techniques for identifying treatment failure. *Invest Radiol*. 2011;46:390–400.

96. Mangla R, Singh G, Ziegelitz D, et al. Changes in relative cerebral blood volume 1 month after radiation-temozolomide therapy can help predict overall survival in patients with glioblastoma. *Radiology*. 2010;256:575–584.
97. Gahramanov S, Muldoon LL, Varallyay CG, et al. Pseudoprogression of glioblastoma after chemo- and radiation therapy: diagnosis by using dynamic susceptibility-weighted contrast-enhanced perfusion MR imaging with ferumoxytol versus gadoteridol and correlation with survival. *Radiology*. 2013;266: 842–852.
98. Yeung TP, Wang Y, He W, et al; Project of Emilia-Romagna Region on Neuro-Oncology Study Group. Survival prediction in high-grade gliomas using CT perfusion imaging. *J Neurooncol*. 2015;123(1):93–102.
99. Batchelor TT, Sorensen AG, di Tomaso E, et al. AZD2171, a pan-VEGF receptor tyrosine kinase inhibitor, normalizes tumor vasculature and alleviates edema in glioblastoma patients. *Cancer Cell*. 2007;11:83–95.
100. Vidiri A, Pace A, Fabi A, et al. Early perfusion changes in patients with recurrent high-grade brain tumor treated with bevacizumab: preliminary results by a quantitative evaluation. *J Exp Clin Cancer Res*. 2012;31:33.
101. Port RE, Bernstein LJ, Barboriak DP, Xu L, Roberts TP, van Bruggen N. Noncompartmental kinetic analysis of DCE-MRI data from malignant tumors: application to glioblastoma treated with bevacizumab. *Magn Reson Med*. 2010; 64:408–417.
102. Ferl GZ, Xu L, Friesenhahn M, Bernstein LJ, Barboriak DP, Port RE. An automated method for nonparametric kinetic analysis of clinical DCE-MRI data: application to glioblastoma treated with bevacizumab. *Magn Reson Med*. 2010;63:1366–1375.
103. Takano S, Kimu H, Tsuda K, et al. Decrease in the apparent diffusion coefficient in peritumoral edema for the assessment of recurrent glioblastoma treated by bevacizumab. *Acta Neurochir Suppl*. 2013;118:185–189.
104. Kreisl TN, Zhang W, Odia Y, et al. A phase II trial of single-agent bevacizumab in patients with recurrent anaplastic glioma. *Neuro Oncol*. 2011;13:1143–1150.
105. Sawlani RN, Raizer J, Horowitz SW, et al. Glioblastoma: a method for predicting response to antiangiogenic chemotherapy by using MR perfusion imaging—pilot study. *Radiology*. 2010;255:622–628.
106. Sorensen AG, Batchelor TT, Zhang WT, et al. A "Vascular normalization index" as potential mechanistic biomarker to predict survival after a single dose of cediranib in recurrent glioblastoma patients. *Cancer Res*. 2009;69:5296–5300.
107. Cabrera AR, Cuneo KC, Desjardins A, et al. Concurrent stereotactic radiosurgery and bevacizumab in recurrent malignant gliomas: a prospective trial. *Int J Radiat Oncol Biol Phys*. 2013;86:873–879.
108. LaViolette PS, Cohen AD, Prah MA, et al. Vascular change measured with independent component analysis of dynamic susceptibility contrast MRI predicts bevacizumab response in high-grade glioma. *Neuro Oncol*. 2013;15:442–450.
109. Schmainda KM, Zhang Z, Prah M, et al. Dynamic susceptibility contrast MRI measures of relative cerebral blood volume as a prognostic marker for overall survival in recurrent glioblastoma: results from the ACRIN 6677/RTOG 0625 multicenter trial. *Neuro Oncol*. 2015;17:1148–1156.
110. Yeung TPC, Yartsev Y, Lee, TY, et al. Relationship of computed tomography perfusion and positron emission tomography to tumour progression in malignant glioma. *J Med Radiat Sci*. 2014;61:4–13.